RESEARCH ARTICLE
SPACE PHYSICS: MAGNETOSPHERIC PHYSICS

Earth and Planetary Physics
3: 8–16, 2019
doi: 10.26464/epp2019002

Magnetosphere response to the IMF turning from north to south

JianYong Lu[1*], HanXiao Zhang[1], Ming Wang[1], ChunLi Gu[2], and HaiYan Guan[3]

[1]Institute of Space Weather, School of Math & Statistics, Nanjing University of Information Science & Technology, Nanjing 210044, China;

[2]Beijing Institute of Applied Meteorology, Beijing 100029, China;

[3]School of Remote Sensing & Geomatics Engineering, Nanjing University of Information Science & Technology, Nanjing 210044, China

Abstract: In this paper, the Space Weather Modeling Framework (SWMF) is used to simulate the real-time response of the magnetosphere to a solar wind event on June 5, 1998, in which the interplanetary magnetic field shifted its direction from north to south. Since most current models do not take into account convective effects of the inner magnetosphere, we first study the importance of Rice Convection Model (RCM) in the global model. We then focus on the following four aspects of the magnetosphere's response: the magnetosphere's density distribution, the structure of its magnetic field lines, the area of the polar cap boundary, and the corresponding ionospheric current change. We find that (1) when the IMF changes from north to south in this event, high magnetosheath density is observed to flow downstream along the magnetopause with the solar wind; low-latitude reconnection at dayside occurs under the southward IMF, while the magnetic field lines in the tail lobe caudal, caused by the nightside high latitude reconnection, extend into the interplanetary space. Open magnetic field lines exist simultaneously at both high and low latitudes at the magnetopause; (2) the area of the polar cap is obviously increased if the IMF turns from the north to the south; this observation is highly consistent with empirical observations; (3) the ionospheric field align current in the northern hemisphere is stronger than in the southern hemisphere and also increases as the IMF changes from north to south. SWMF with the Rice Convection effect provides reliable modeling of the magnetospheric and ionospheric response to this solar wind variation.

Keywords: magnetosphere; global MHD simulation; polar cap; magnetic reconnection

Citation: Lu, J. Y., Zhang, H. X., Wang, M., Gu, C. L., and Guan, H. Y. (2019). Magnetosphere response to the IMF turning from north to south. *Earth Planet. Phys.*, *3*(1), 8–16. http://doi.org/10.26464/epp2019002

1. Introduction

The interplanetary magnetic field (IMF) plays an important role in the magnetosphere-ionosphere coupling and is likely to reconnect with the geomagnetic field in any direction. In the southward direction of the IMF, the reconnection occurs near the equatorial plane at the magnetopause, and the reconnection rate is the largest. When the IMF is northward, the magnetic reconnection occurs near the caudal lobe behind the polar cusp, and the reconnection becomes weakest (eg., Luhmann et al., 1984; Shepherd et al., 2002; Lu JY et al., 2013a). It is found that if the polar cap electric potential difference is equivalent to the magnetic reconnection rate, the reconnection rate under the northward IMF in the solar wind-magnetosphere coupling is about 10%–13% of that in the southward IMF (Jing H et al., 2014).

Russel and Elphic (1978) found, from ISEE 1/2 satellite data, that in and near the low-latitude magnetopause, the magnetic field, plasma, and high-energy particles often exhibit a kind of equal-scale perturbation that lasts for 1–2 min and repeats every 6–9 min, accompanied by magnetic flux transmission and plasma flow enhancement, i.e. flux transfer events, which they believe are related to the instantaneous magnetic field reconnection. In recent years, the more and more energy transmission caused by the northward interplanetary magnetic field has also been observed (e.g., Shi QQ et al., 2013; Gou XC et al., 2016). Shi et al. (2009), using Cluster satellite observation data, found that solar wind particles entering the magnetosphere from the magnetic sheath were detected near the polar cusp region in the northward IMF condition. The polar cusp is like the window of the magnetosphere, a critical area where the solar wind energy enters the magnetosphere. They speculate this may be related to the magnetic reconnection behind the tail valve. Raeder et al. (2000) compared output of the global geospace circulation model (GGCM) with observations made from low-latitude spacecraft at the settlement boundary and found that the simulated particle sedimentation boundary was in good agreement with local observations except for the dusk side. Feldman et al. (1995) found that particle sedimentation was observed in the polar cap region when the IMF made a sharp turn to the morning-north direction. Øieroset et al. (2005) and Yang YF et al. (2011) found that high-latitude dayside aurora occur under conditions where the IMF is northward. Korth et al. (2005) found that electromagnetic energy flow and particle sedimentation were observed in a small area of the magnetic pole region under the condition of strong lasting northward IMF. Moreover, Knipp et al. (2011) and Li et al. (2011) also found that the DMSP F15 satellite often observes electromagnetic energy flow near the polar region under the northward IMF condition,

Correspondence to: J. Y. Lu, jylu@nuist.edu.cn
Received 01 OCT 2018; Accepted 11 DEC 2018.
Accepted article online 28 DEC 2018.
©2019 by Earth and Planetary Physics.

with a large B_y component. Raeder et al. (2000) used the GGCM to model an observed substorm, finding that a substorm could not be triggered without explosive reconfigurations of the magnetic field lines. Wang JY et al. (2014) used a global MHD model to show that the effects of the interplanetary magnetic field can even result in a twisting of the magnetotail.

Obviously, the solar wind-magnetosphere-ionosphere coupling is complex, especially during the turning of IMF directions. The coupling involves the dynamic processes of energy entry to the magnetosphere, magnetospheric density variation and geomagnetic structure change, substorm triggering, ionospheric current generation, and so on. It is beneficial to investigate these processes to better understand the underlying physics involved. Computer simulation provides a useful tool; global simulations are playing a more and more important role in studies of this coupling (e.g., Ogino, 1986; Gombosi et al., 2000; García and Hughes, 2007; Wang JY et al., 2014). However, lack of global observational data limits most of the results to point to point comparison between magnetosphere models and satellite data (e.g., Fedder et al., 1995); thus the effectiveness of the large-scale MHD model is yet to be more empirically confirmed. The open and closed boundary closely related to the dynamics of store and release during the substorm can be used as such a testing tool for the effectiveness of numerical simulation. For the first time Rae et al. used the Space Weather Modeling Frame-work (SWMF, Tóth et al., 2005)) with the Rice convection model (RCM) to compare the boundary of open and closed magnetic field with CANOPUS's point measurements for all MLT to the event on June 5, 1998 (Rae et al., 2010). However, the dynamic response of the magnetosphere to the north-south turning IMF has not been analyzed in detail. As a supplement, we continue to use this event to show the response of a magnetosphere to the IMF north-south turning, because the north-south transition of the IMF in this event is sudden and frequent, triggering a series of magnetospheric substorms.

The paper is organized as follows. In Section 2 we introduce the data and model used in this research. Section 3 presents the MHD simulation results of magnetosphere response to a specific solar wind event, and Section 4 gives the summary and conclusion.

2. Data and Model

The real time upstream solar wind parameters are from OMNI data (http://cdaweb.gsfc.nasa.gov/cgi-bin/eval1.cgi). This strongly disturbed solar wind will inevitably interfere with the magnetosphere, and the response of the magnetosphere and ionosphere will be given in the model results. The corresponding geomagnetic data (shown below) are from the Kyoto Geomagnetic Center, which is part of the World Data Center.

Figure 1 shows the solar wind observations on June 5, 1998, at 11:00–17:00 UT from ACE (solid) and WIND (dashed), and the *Kp*

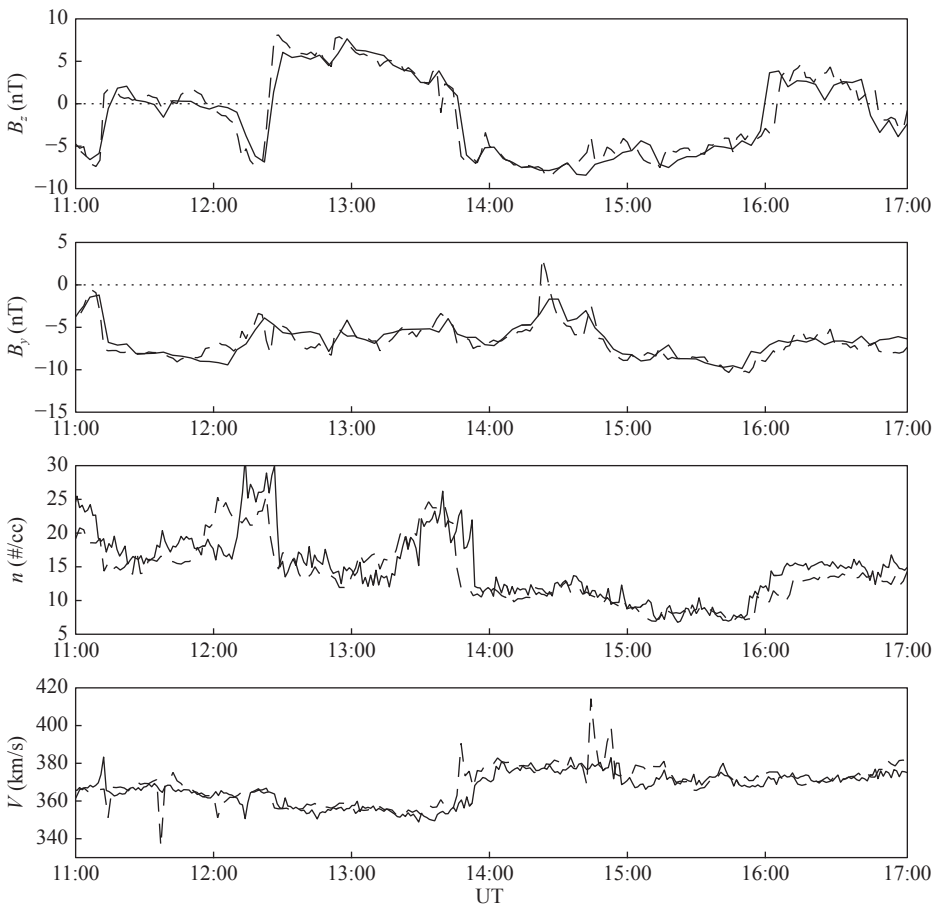

Figure 1. Solar wind observations from ACE (solid) and WIND (dashed) on June 5, 1998, observed from 11:00–17:00 UT. The solar winds observed by the two spacecraft are quite consistent, indicating that the direction of the interplanetary magnetic field is accurate.

index. Comparison of the solar wind observations made by the two spacecrafts shows them to be quite consistent; that is, the observed values of the interplanetary parameters appear to be accurate. Note that the two spacecraft reached the magnetopause with a time delay of 66 and 78 minutes respectively, which is already considered in this research. During the period from 12:00–14:30 UT in this event, the interplanetary magnetic field has two obvious north-south direction transitions in a short time: at 12:10 UT, the IMF began to turn southward (the first turning) but did not do so for long; at about 12:25 UT, the IMF suddenly turned from south to north. After maintaining northward orientation for more than an hour, the IMF suddenly turned southward again at about 13:45 UT, followed by a period of relatively stable solar wind.

During this observation, except for several small disturbances, the B_y component of the interplanetary magnetic field was relatively stable, at about −5 nT. Before the second southward turn at 13:50 UT, the solar wind speed was about 350–360 km/s, but as the interplanetary magnetic field suddenly turned southward, the solar wind speed began to increase to 370–380 km/s, and then did not change much. The density of the solar wind increased suddenly during these two turns. When the interplanetary magnetic field became stabilized, however, the density, too, changed very little. It should be mentioned that as usual the B_x is taken to be zero in the calculation to avoid the problem of non-zero divergence of the magnetic field. It should be mentioned that the dipole tilt angles gradually increased from 22:38° at 11:00 UT to 32:73° at 17:00 UT.

The SWMF is a well developed suite of computational models that can be used for modeling physical processes from the Sun to the Earth (e.g., De Zeeuw et al., 2004; Tóth et al., 2005). The SWMF consists of several numerical modules, the ideal MHD solver (BATS-R-US) (Powell et al., 1999), the ionospheric electrodynamics (IE) model (Ridley et al., 2002), and the Rice Convection Model (RCM) (Toffoletto et al., 2003). The SWMF has been used extensively to study various solar wind influences on the magnetosphere, for example, northward IMF (Song P et al., 1999; Watanabe et al., 2005; Lu JY et al., 2011), IMF B_y effects (e.g., Kabin et al., 2003; Lu et al., 2013a), dipole tilt effects (Liu ZQ et al., 2012), and Parker spiral angles (Gombosi et al., 2000). The SWMF configuration including a fully coupled RCM module has been used, for example, for southward IMF (De Zeeuw et al., 2004), storm dynamics (Zhang JC et al., 2007; Tóth et al., 2007); and energy transport through the magnetopause (Lu JY et al., 2013b; Jing H et al., 2014). In this paper we use the BATS-R-US, IE, and RCM coupled model. The computational domain is defined by $-70\ R_E \leq X \leq 20\ R_E$, $-60\ R_E \leq Y, Z \leq 60\ R_E$, with grid size of 1.25 R_E. Inside $-40\ R_E \leq X \leq 20\ R_E$ and $-45\ R_E \leq Y, Z \leq 45\ R_E$, the grid size is 0.625 R_E, and inside $-25\ R_E \leq X \leq 12.5\ R_E$, and $-30\ R_E \leq Y, Z \leq 30\ R_E$, the grid size is 0.3125 R_E. The inner boundary is a sphere at 2.5 R_E. The real time upstream solar wind parameters of ACE from OMNI data are the inputs of the SWMF.

3. Results

Since most of the current global models do not take into account the effects of magnetosphere convection, we first investigate the effect of convection upon the magnetosphere with and without the Rice convection. Figure 2 shows the magnetic field and pressure contour in the meridional plane at 11:30 UT (at this time the interplanetary magnetic field is northward) (Figures 2a–2b) and 12:10 UT (south direction of interplanetary magnetic field) (Figures 2c–2d), respectively. The left panel (Figure 2a and 2c) corresponds to the result with Rice Convection effect, and the right (Figures 2b and 2d) without Rice convection. It can be seen that when the interplanetary magnetic field is northward (Figures 2a–2b), the maximum pressure value (about 2.7 nPa) is located in the cusp area and the pressure in the loop current is less than 1 nPa in the case of no convection (Figure 2b); but if Rice convection is included (Figure 2a), the maximum pressure (3.7 nPa) is in the loop current at approximately 6 R_E and the reconnected X line is pushed away from the Earth. Obviously, the model correctly reflects the convection effect. This should also be the case when the interplanetary magnetic field is southward.

In the case of no Rice Convection (Figure 2d), the maximum pressure value 2.9 nPa is in the cusp and the pressure in the ring current is less than 1 nPa; with Rice Convection (Figure 2c), however, the maximum pressure (about 2.4 nPa) goes to the ring current zone, but the pushing away reconnected X line is not obvious because of the influence of changing solar wind. Note that the maximum ring current pressure (at 12:10 UT in Figure 2d, although at this time the IMF is southward) is smaller than the maximum ring current pressure in Figure 2c when IMF is northward, which does mean that the ring current in the northward IMF is stronger than in the southward. Our calculation uses real-time solar wind input, so the results under different solar wind conditions cannot be compared. The influence of magnetosphere convection on the pressure and magnetic field of the inner magnetosphere should undoubtedly be taken into consideration in the global simulation, especially for investigations of substorm and polar cap boundaries.

In the following we introduce our results for the real-time simulation of the response of magnetosphere and ionosphere to the 5 June 1998 event, taking into account the contribution of the Rice convection effect.

Figure 3 is the contour of magnetospheric density in the *XZ* plane obtained from the SWMF at 11:30, 12:10, 13:20 UT, and 14:00 UT, respectively. The directions of the IMF at these four times are: morning direction, morning-south direction, morning-north direction, and morning-south direction. It can be seen from the figure that the solar wind conditions at the beginning stage change little, and the physical disturbance such as the magnetosheath density is small. At 12:10 UT, the shock wave reaches the magnetopause dayside; the density of the nearby magnetosheath becomes large, and the magnetosphere is compressed. The high magnetosheath density then flows downstream along the magnetopause with the solar wind. It can be seen from the magnetic field lines in Figure 3c that the IMF is connected to the Earth's magnetic field at high latitudes, which is an open magnetic field structure, and the nearby subsolar region exhibits closed magnetic field lines. In Figures 3b and 3d, the upstream magnetic field (the southward IMF on the Sunside) moves downstream by following the northward IMF moving to the night side; also shown in the figure are signs of reconnection between the IMF and the geo-

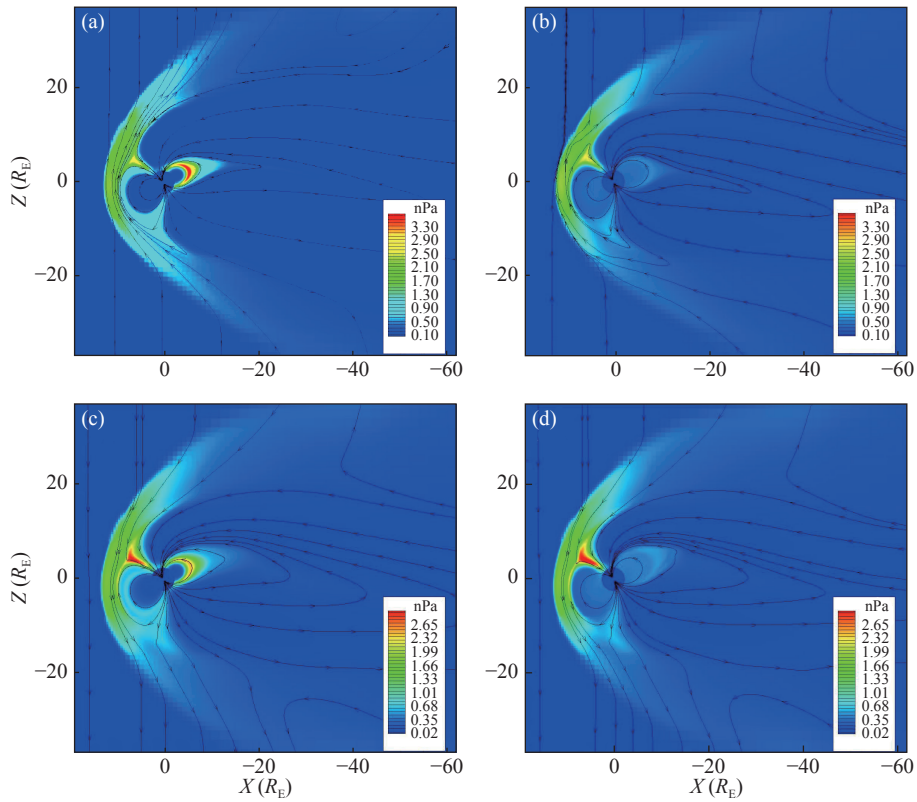

Figure 2. The magnetic field lines and pressure contour in the *XZ* plane with Rice convection (a) and (c) and without Rice convection (b) and (d) at 11:30 UT (a, b) and at 12:10 UT (c, d), respectively. The IMFs in Figures 2a and 2b are northward, while in Figures 2c and 2d they are southward.

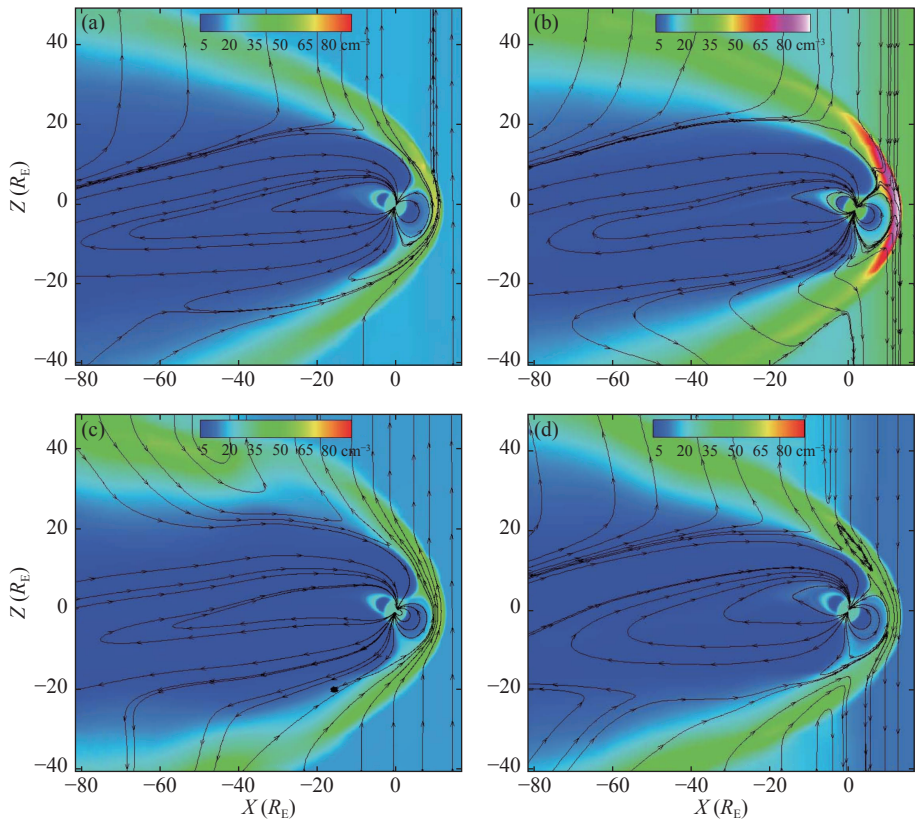

Figure 3. The magnetic field lines and density contour in the *XZ* plane at 11:30 UT (a), 12:10 UT (b), 13:20 UT (c), and 14:00 UT (d). The black vector line represents the magnetic field line.

magnetic field in different directions. At the dayside, the low-latitude reconnection occurs under the southward IMF, while the magnetic field lines in the tail lobe caudal caused by the nightside high latitude reconnection extend into the interplanetary space. There exist open magnetic field lines simultaneously at both high and low latitudes at the magnetopause; that is, the low latitude reconnection starts, and the high latitude reconnection has not yet ended.

The boundary of the open and closed magnetic field lines (polar cap boundary) corresponding to the storage and release of magnetic energy during a substorm is found. Figure 4 shows the polar cap size (blue) of the ionosphere in the northern hemisphere (left) and the southern hemisphere (right) under northward IMF (top), southward IMF (middle), and southward IMF (bottom) conditions, respectively. It is found that: (1) at the same time, the polar cap area in the southern hemisphere is larger than that in the northern hemisphere; (2) as the interplanetary magnetic field changes from north to south, the polar cap area also increases. This is because when the interplanetary magnetic field has a southward component, the interplanetary magnetic field will reconnect with the closed magnetic field line on the dayside, opening a new flow tube; the polar cap area is thus increased. However, when the interplanetary magnetic field is northward, the magnetic field lines on the night side will reconnect, the flow tubes in the open area will be destroyed, and the boundary area of the polar cap will become smaller. Milan et al. (2003) used empirical data from the SuperDARN HF radar, the Polar UVI Imager, and the particle detectors of low Earth orbit spacecraft to determine the OCB with the change of MLT, and found that the change of the open magnetic

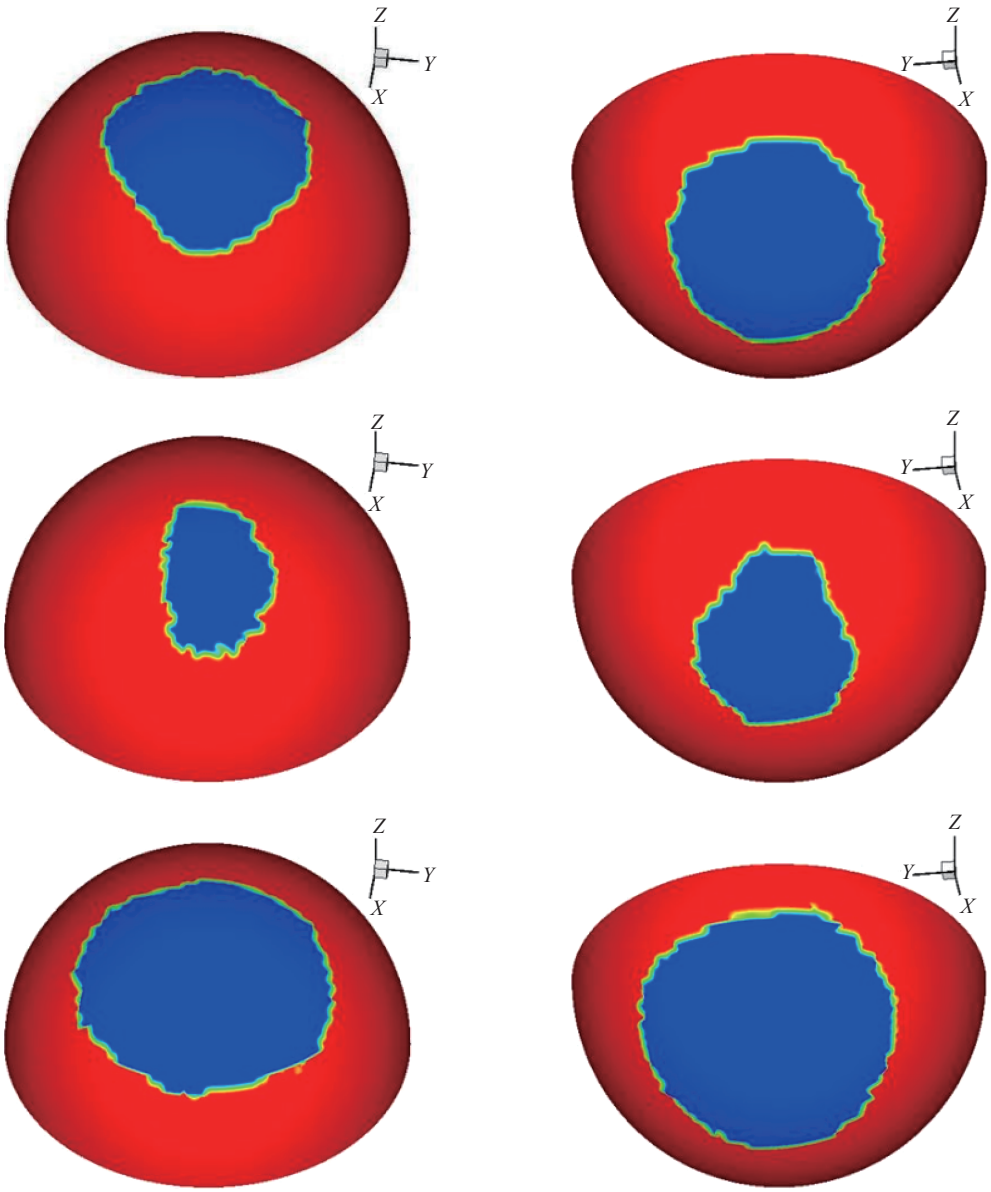

Figure 4. The color line indicates the polar cap boundary of the ionosphere in the northern hemisphere (left) and the southern hemisphere (right) with Rice Convection considered in the SWMF global model. The top, middle, and bottom charts are at 13:38 UT (northward IMF), 14:18 UT (southward IMF), and 14:28 UT (southward IMF), respectively.

field in the magnetosphere is directly related to the balance of the magnetic reconnections between dayside and nightside. When the IMF is in the south, the opening area increases and then becomes smaller when the sudden commencement of the substorm expansion phase is triggered. Obviously, our result agrees well with Milan et al. (2003).

Figure 5 compares the modelled and the observed OCB at 14:57 UT (southward IMF). Figure 5 also show a Polar UV image (gray scale); backscatter was observed simultaneously from three of the six SuperDARN HF radars for clarity (in color). The red line and black circles are the model and observation-derived OCBs, respectively. The observed OCB was determined by taking the poleward edge of high-energy (1–10 keV) electron precipitation (e.g., Evans and Stone, 1972), while the equatorward edge of the ~250 m/s Super-DARN spectral widths and the poleward gradient in Polar UVI emissions are employed as proxies for the OCB on the dayside and nightside, respectively. For brevity, particle precipitation boundaries, that were also used to determine the observed OCB, are not shown (see Milan et al., 2003 for details) but are included in the observational estimate of the OCB. At 13:37 UT, when the IMF is northward, there is near-perfect agreement on the dayside, but in the postmidnight to dawn sector, there is some difference. At 14:57 UT, when the IMF is southward, the modelled OCBs agree very well with the observed. These results show that the global model, SWMF+RICE, can provide useful and reliable magnetic fields and identify open and closed boundaries.

Figure 6a shows the three-dimensional shape of the last closed magnetic field line at 13:37 UT (northward IMF). Figure 6b is the set of magnetic field lines after the IMF turns southward at 14:57 UT; the color contour represents the density. It can be seen that, just as we analyzed above, the closed geomagnetic field line (red) under the northward IMF is open (white) and reconnected with

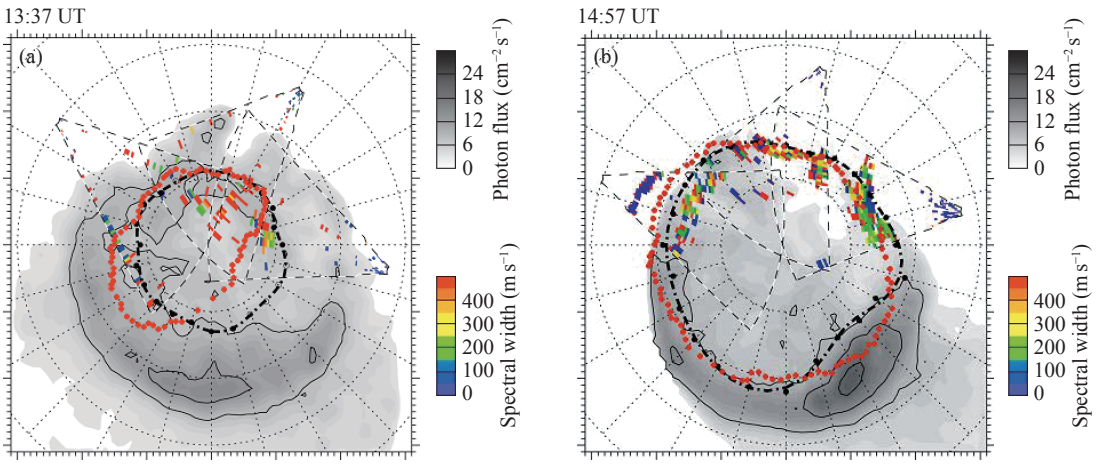

Figure 5. Comparison of the observed and modelled OCBs at 13:37 UT (a) and 14:57 UT (b). Also shown are plots of Polar UVI auroral intensity (gray scale) and SuperDARN HF radar spectral widths (color scale) in magnetic latitude (MLAT): magnetic local time (MLT) coordinates. Dotted circles show 60°, 70°, and 80° MLAT, and radial lines are MLT meridians, with noon at the top of the page. The dash-dotted line and circles are the observed data, and the red dashed line is the modelled result. Filled circles represent MLT sectors derived from available observational OCB measurements; if there were no nearby measurements, the OCB is interpolated from earlier and later MLTs and shown by open circles. Figure 5a shows the comparison at 13:37 UT under northward IMF conditions. Figure 5b shows the comparison at 14:57 UT after the southward IMF turning.

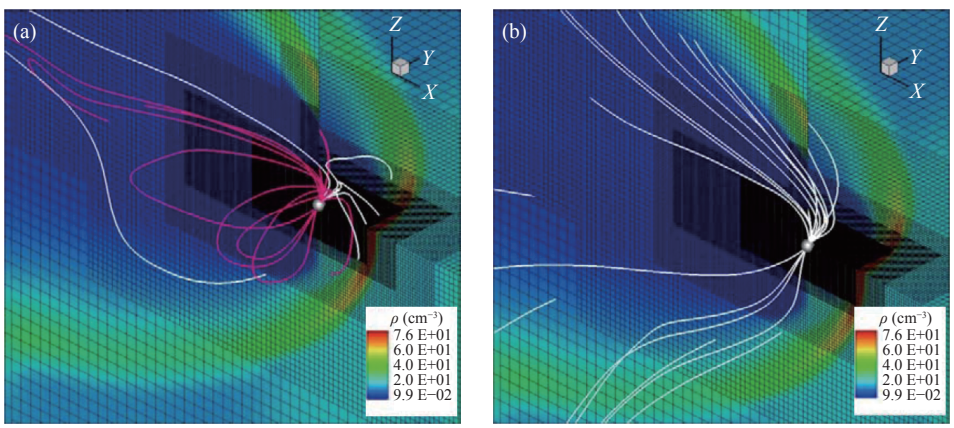

Figure 6. The last closed magnetic field lines (red) at 13:37 UT (northward IMF) (a) are opened and reconnected with IMF at 14:57 UT after the IMF turns southward (b). The red line shows the closed magnetic field lines and the white shows open field lines.

the IMF when the IMF turns southward.

Figure 7 shows the ionospheric field aligned currents of the northern (a and c) and southern (b, d) hemispheres at 13:37 UT (northward IMF, a and b) and at 14 :57 UT (southward IMF, c and d), respectively. Comparing these demonstrates that: (1) at the same time, the ionospheric current of the northern hemisphere is stronger than that of the southern hemisphere; (2) when the interplanetary magnetic field changes from north to south, the ionospheric field align current (especially in the northern hemisphere) obviously increases. The asymmetries in field aligned current intensity and polar cap area in Figure 4 between southern and northern hemispheres are caused by the dipole tilt effect. The magnetopause, magnetic field structure, magnetotail currents, field align currents, and polar cap area or cusp all depend on the dipole tilt angle (e.g., Newell and Meng CI, 1989; Tsyganenko and Stern, 1996). Specifically, Guo JG et al. (2013) pointed out that the effect of dipole tilt angle on the cusp is asymmetric in the northern and southern hemispheres and this impact on the southern hemisphere cusp is smaller than on the northern hemisphere cusp. For the event we investigate, the dipole tilt angle gradually increases from 22:38° at 11:00 UT to 32: 73° at 17:00 UT. For positive tilt angles, more solar wind particles easily enter the north hemisphere ionosphere because of the distorted magnetopause current systems, and it is easily understood to ascribe the asymmetries of field align currents and polar caps between southern and northern hemisphere to ionospheric conductivity changes associated with the effects of dipole tilt angle.

4. Summary and Conclusions

In the solar wind event of June 5, 1998 selected for analysis in this paper, the interplanetary magnetic field has two obvious north-to-south transitions in a relatively short period of time, so that we can specifically study the real-time response of the magnetosphere and the ionosphere during IMF turning related to the tremendous energy input to the magnetosphere. Taking the solar wind observation data as real time input, we use the global magnetospheric model, SMWF, to simulate the magnetosphere and ionosphere response to this special event. We first study the importance of Rice Convection in the global model, then discuss the magnetospheric and ionospheric responses to the 5 June 1998

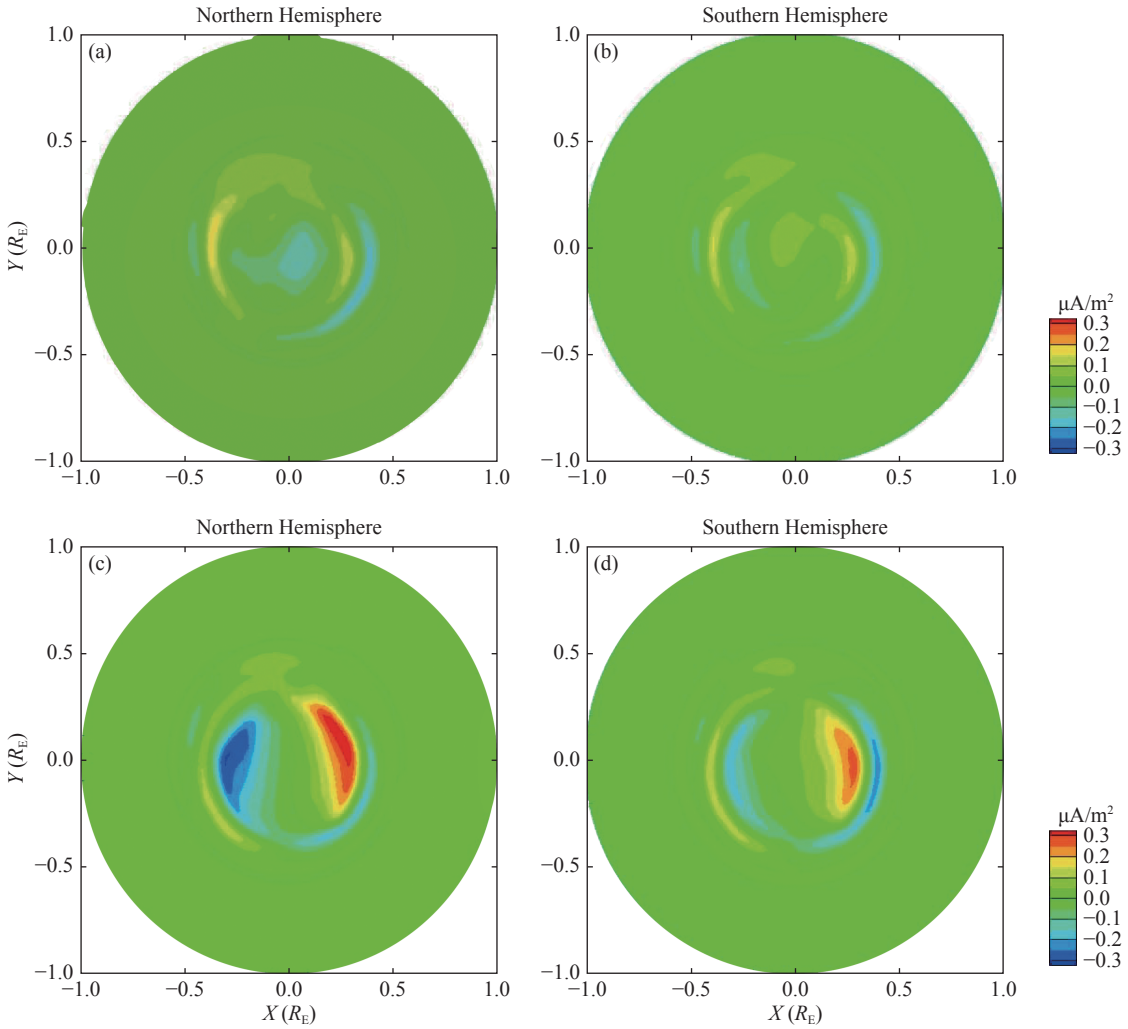

Figure 7. The ionospheric field align currents in the northern hemisphere (a, c) and southern hemisphere (b, d) at 13:37 UT (northward IMF, a and b) and at 14 :57 UT (southward IMF, c and d).

solar wind event. The main results are summarized as follows:

(1) When IMF changes from north to south in this event, high magnetosheath density is observed to flow downstream along the magnetopause with the solar wind, the low-latitude reconnection at dayside occurs under the southward IMF, while the magnetic field lines in the tail lobe caudal caused by the nightside high latitude reconnection extend into the interplanetary space. There exist open magnetic field lines simultaneously at both high and low latitudes at the magnetopause.

(2) The area of polar cap can be used to characterize the effect of IMF turning from the north to the south. The area of the polar cap is obviously increased if the IMF turns from the north to the south, because the southward IMF reconnects with the closed geomagnetic field in the dayside, the new magnetic flux tube is opened, and this increases the boundary area of the polar cap. When the IMF is northward, the magnetic field line on the night side will reconnect to the IMF, and the flux tube is broken so that the boundary area of the polar cap becomes smaller.

(3) The ionospheric field align current in the northern hemisphere is stronger than in the southern hemisphere and will also increase as the IMF changes from north to south.

(4) The SWMF can reproduce the response of the magnetosphere and the ionosphere to solar wind events, and can provide useful and reliable magnetic fields and open and closed boundaries.

Acknowledgments.

This work was supported in part by the National Natural Science Foundation of China (grant 41574158, U 1631107, 41604141), the Jiangsu Shuangchuang Program, and the Natural Science Foundation of Jiangsu Province (Youth Fund: No. BK20160952, BK20140993).

References

De Zeeuw, D. L., Sazykin, S., Wolf, R. A., Gombosi, T. I., Ridley, A. J., and Tóth, G. (2004). Coupling of a global MHD code and an inner magnetospheric model: Initial results. *J. Geophys. Res.*, *109*(A12), A12219. https://doi.org/10.1029/2003JA010366

Evans, L. C., and Stone, E. C. (1972). Electron polar cap and the boundary of open geomagnetic field lines. *J. Geophys. Res.*, *77*(28), 5580–5584. https://doi.org/10.1029/JA077i028p05580

Fedder, J. A., and Lyon, J. G. (1995). The Earth's magnetosphere is 165 R_E long: Self-consistent currents, convection, magnetospheric structure, and processes for northward interplanetary magnetic field. *J. Geophys. Res.*, *100*(A3), 3623–3635. https://doi.org/10.1029/94JA02633

Feldman, W. C., Hones, E. W., Barraclough, B. L., Reeves, G. D., Belian, R. D., Cayton, T. E., Lee, P., Lepping, R. P., Trombka, J. I., …Rich, F. J. (1995). Possible conjugate reconnection at the high-latitude magnetopause. *J. Geophys. Res.*, *100*(A8), 14913–14923. https://doi.org/10.1029/95JA01217

García, K. S., and Hughes W. J. (2007). Finding the Lyon-Fedder-Mobarry magnetopause: A statistical perspective. *J. Geophys. Res.*, *112*(A6). https://doi.org/10.1029/2006JA012039

Gombosi, T. I., DeZeeuw, D. L., Groth, C. P. T., and Powell, K. G. (2000). Magnetospheric configuration for Parker-spiral IMF conditions: results of a 3D AMR MHD simulation. *Adv. Space Res.*, *26*(1), 139–149. https://doi.org/10.1016/S0273-1177(99)01040-6

Gou, X. C., Shi, Q. Q., Tian, A. M., Sun, W. J., Dunlop, M. W., Fu, S. Y., Zong, Q. G., Facskó, G., Nowada, M., … Shen, X. C. (2016). Solar wind plasma entry observed by cluster in the high-latitude magnetospheric lobes. *J. Geophys. Res.*, *121*(5), 4135–4144. https://doi.org/10.1002/2015JA021578

Guo, J. G., Shi, J. K., Cheng, Z. W., Zhang, Z. Y., Wang, Z., Zhang, T. L., Liu, Z. X., and Dunlop, M. (2013). Variation of dependence of the cusp location at different altitude on the dipole tilt. *Chin. Sci. Bull.*, *58*(28-29), 3541–3545. https://doi.org/10.1007/s11434-013-5831-1

Jing, H., Lu, J. Y., Kabin, K., Zhao, J. S., Liu, Z. Q., Yang, Y. F., Zhao, M. X., and Wang, M. (2014). MHD simulation of energy transfer across magnetopause during sudden changes of the IMF orientation. *Planet. Space Sci.*, *97*, 50–59. https://doi.org/10.1016/j.pss.2014.04.001

Kabin, K., Rankin, R., Marchand, R., Gombosi, T. I., Clauer, C. R., Ridley, A. J., Papitashvili, V. O., and DeZeeuw, D. L. (2003). Dynamic response of Earth's magnetosphere to B_y reversals. *J. Geophys. Res.*, *108*(A3), 1132. https://doi.org/10.1029/2002JA009480

Knipp, D., Eriksson, S., Kilcommons, L., Crowley, G., Lei, J., Hairston, M., and Drake, K. (2011). Extreme poynting flux in the dayside thermosphere: Examples and statistics. *Geophys. Res. Lett.*, *38*(16), L16102. https://doi.org/10.1029/2011GL048302

Korth, H., Anderson, B. J., Frey, H. U., and Waters, C. L. (2005). High-latitude electromagnetic and particle energy flux during an event with sustained strongly northward IMF. *Ann. Geophys.*, *23*(4), 1295–1310. https://doi.org/10.5194/angeo-23-1295-2005

Li, W., Knipp, D., Lei, J., and Raeder, J. (2011). The relation between dayside local Poynting flux enhancement and cusp reconnection. *J. Geophys.Res.*, *116*(A8), A08301. https://doi.org/10.1029/2011JA016566

Liu, Z. Q., Lu, J. Y., Kabin, K., Yang, Y. F., Zhao, M. X., and Cao, X. (2012). Dipole tilt control of the magnetopause for southward IMF from global magnetohydrodynamic simulations. *J. Geophys. Res.*, *117*(A7), A07207. https://doi.org/10.1029/2011JA017441

Lu, J. Y., Liu, Z. Q., Kabin, K., Zhao, M. X., Liu, D. D., Zhou, Q., and Xiao, Y. (2011). Three dimensional shape of the magnetopause: Global MHD results. *J. Geophy. Res.*, *116*(A9), A09237. https://doi.org/10.1029/2010JA016418

Lu, J. Y., Liu, Z. Q., Kabin, K., Jing, H., Zhao, M. X., and Wang, Y. (2013a). The IMF dependence of the magnetopause from global MHD simulations. *J. Geophys. Res.*, *118*(6), 3113–3125. https://doi.org/10.1002/jgra.50324

Lu, J. Y., Jing, H., Liu, Z. Q., Kabin, K., and Jiang, Y. (2013b). Energy transfer across the magnetopause for northward and southward interplanetary magnetic fields. *J. Geophys. Res.*, *118*(5), 2021–2033. https://doi.org/10.1002/jgra.50093

Luhmann, J. G., Walker, R. J., Russell, C. T., Crooker, N. U., Spreiter, J. R., and Stahara, S. S. (1984). Patterns of potential magnetic field merging sites on the dayside magnetopause. *J. Geophys. Res.*, *89*(A3), 1739–1742. https://doi.org/10.1029/JA089iA03p01739

Milan S. E., Lester M., Cowley S. W. H., Oksavik, K., Brittnacher, M., Greenwald, R. A., Sofko, G., and Villain, J. P. (2003). Variations in the polar cap area during two substorm cycles. *Ann. Geophys.*, *21*(5), 1121–1140. https://doi.org/10.5194/angeo-21-1121-2003

Newell, P. T., and Meng, C. I. (1989). Dipole tilt angle effects on the latitude of the cusp and cleft/low- altitude boundary layer. *J. Geophys. Res.*, *94*(A6), 6949–6953. https://doi.org/10.1029/JA094iA06p06949

Ogino, T. (1986). A three-dimensional MHD simulation of the interaction of the solar wind with the Earth's magnetosphere: the generation of field-aligned currents. *J. Geophys. Res.*, *91*(A6), 6791–6806. https://doi.org/10.1029/JA091iA06p06791

Øieroset, M., Raeder, J., Phan, T. D., Wing, S., McFadden, J. P., Li, W., Fujimoto, M., Rème, H., and Balogh, A. (2005). Global cooling and densification of the plasma sheet during an extended period of purely northward IMF on October 22-24, 2003. *Geophys. Res. Lett.*, *32*(12), L12S07. https://doi.org/10.1029/2004GL021523

Powell, K. G., Roe, P. L., Linde, T. J., Gombosi, T. I., and De Zeeuw, D. L. (1999). A solution- adaptive upwind scheme for ideal magnetohydrodynamics. *J. Comput. Phys.*, *154*(2), 284–309. https://doi.org/10.1006/jcph.1999.6299

Rae, I. J., Kabin, K., Lu, J. Y., Rankin, R., Milan, S. E., Fenrich, F. R., Watt, C. E. J., Zhang, J. C., Ridley, A. J., … DeZeeuw, D. L. (2010). Comparison of the open-closed separatrix in a global magnetospheric simulation with observations: The role of the ring current. *J. Geophys. Res.*, *115*(A8), A08216. https://doi.org/10.1029/2009JA015068

Raeder, J., McPherron, R. L., Frank, L. A., Kokubun, S., Lu, G., Mukai, T., Paterson, W. R., Sigwarth, J. B., Singer, H. J., and Slavin, J. A. (2000). Global simulation of the Geospace Environment Modeling substorm challenge event. *J. Geophys. Res.*, *106*(A1), 381–395. https://doi.org/10.1029/2000JA000605

Ridley, A. J., Hansen, K. C., Tóth, G., De Zeeuw, D. L., Gombosi, T. I., and Powell, K. G. (2002). University of Michigan MHD results of the geospace global circulation model metrics challenge. *J. Geophys. Res.*, *107*(A10), 1290. https://doi.org/10.1029/2001JA000253

Russell, C. T., and Elphic, R. C. (1978). Initial ISEE magnetometer results: Magnetopause observations. *Space Sci. Rev.*, *22*(6), 681–715. https://doi.org/10.1007/BF00212619

Shepherd, S. G., Greenwald, R. A., and Ruohoniemi, J. M. (2002). Cross polar cap potentials measured with Super Dual Auroral Radar Network during quasi-steady solar wind and interplanetary magnetic field conditions. *J. Geophys. Res.*, *107*(A7), 1094. https://doi.org/10.1029/2001JA000152

Shi, Q. Q., Zong, Q.-G., Zhang, H., Pu, Z. Y., Fu, S. Y., Xie, L., Chen, Y., Li, L., Xia, L. D., Liu, Z. X., Fazakerley, A. N., Reme, H., and Lucek, E. (2009). Cluster observations of the entry layer equatorward of the cusp under northward interplanetary magnetic field. *J. Geophys. Res.*, *114*(A12), A12219. https://doi.org/10.1029/2009JA014475

Shi, Q. Q., Zong, Q. G., Fu, S. Y., Dunlop, M. W., Pu, Z. Y., Parks, G. K., Wei, Y., Li, W. H., Zhang, H., … Lucek, E. (2013). Solar wind entry into the high-latitude terrestrial magnetosphere during geomagnetically quiet times. *Nat. Commun.*, *4*, 1466. https://doi.org/10.1038/ncomms2476

Song, P., DeZeeuw, D. L., Gombosi, T. I., Groth, C. P. T., and Powell, K. G. (1999). A numerical study of solar wind-magnetosphere interaction for northward interplanetary magnetic field. *J. Geophys. Res.*, *104*(A12), 28361–28378. https://doi.org/10.1029/1999JA900378

Toffoletto, F., Sazykin, S., Spiro, R., and Wolf, R. (2003). Inner magnetospheric modeling with the Rice Convection Model. *Space Sci. Rev.*, *107*(1-2), 175–196. https://doi.org/10.1023/A:1025532008047

Tóth, G., Sokolov, I. V., Gombosi, T. I., Chesney, D. R., Clauer, C. R., de Zeeuw, D. L., Hansen, K. C., Kane, K. J., Manchester, W. B., … Kóta, J. (2005). Space Weather Modeling Framework: A new tool for the space science community. *J. Geophys. Res.*, *110*(A12), A12226. https://doi.org/10.1029/2005JA011126

Tóth, G., De Zeeuw, D. L., Gombosi, T. I., Manchester, W. B., Ridley, A. J., Sokolov, I. V., and Roussev, I. I. (2007). Sun-to-thermosphere simulation of the 28-30 October 2003 storm with the Space Weather Modeling Framework. *Space Wea.*, *5*(6), S06003. https://doi.org/10.1029/2006SW000272

Tsyganenko, N. A., and Stern, D. P. (1996). Modeling the global magnetic field of the large-scale Birkeland current systems. *J. Geophys. Res.*, *101*(A12), 27187–27198. https://doi.org/10.1029/96JA02735

Wang, J. Y., Wang, C., Huang, Z. H., and Sun, T. R. (2014). Effects of the interplanetary magnetic field on the twisting of the magnetotail: Global MHD results. *J. Geophys. Res.*, *119*(3), 1887–1897. https://doi.org/10.1002/2013JA019257

Watanabe, M., Kabin, K., Sofko, G. J., Rankin, R., Gombosi, T. I., Ridley, A. J., and Clauer, C. R. (2005). Internal reconnection for northward interplanetary magnetic field. *J. Geophys. Res.*, *110*(A6), A06210. https://doi.org/10.1029/2004JA010832

Yang, Y. F., Lu, J. Y., Wang, J. S., Peng, Z., Qian, Q., and Xiao, Y. (2011). Different response of dayside auroras to increases in solar wind dynamic pressure. *J. Geophys. Res.*, *116*(A8), A08314. https://doi.org/10.1029/2010JA016385

Zhang, J. C., Liemohn, M. W., de Zeeuw, D. L., Borovsky, J. E., Ridley, A. J., Toth, G., Sazykin, S., Thomsen, M. F., Kozyra, J. U., … Wolf, R. A. (2007). Understanding storm-time ring current development through data-model comparisons of a moderate storm. *J. Geophys. Res.*, *112*(A4), A04208. https://doi.org/10.1029/2006JA011846